Unique nanostructural features in Fe, Mn-doped YBCO thin films

Unique nanostructural features in Fe,Mn-doped YBCO thin films

A. Meledin[1], S. Turner[1], P. Cayado[2], B. Mundet[2], E. Solano[3], S. Ricart[2], J. Ros[3], T. Puig[2], X. Obradors[2] and G. Van Tendeloo[1]

[1]*Electron microscopy for materials science (EMAT), Physics Department, Antwerp University, Antwerp, 2020, Belgium*

[2]*Institut de Ciència de Materials de Barcelona—CSIC, Campus UAB, 08193, Bellaterra, Catalonia, Spain*

[3] *Departament de Química, Facultat de Ciències, Universitat Autònoma de Barcelona, 08193, Bellaterra, Catalonia, Spain*

E-mail: alexander.meledin@uantwerp.be

Abstract

An attempt to grow a thin epitaxial composite film of $YBa_2Cu_3O_{7-\delta}$ (YBCO) with spinel $MnFe_2O_4$ (MFO) nanoparticles on a LAO substrate using the CSD approach resulted in a decomposition of the spinel and various doping modes of YBCO with the Fe and Mn cations. These nanostructural effects lead to a lowering of Tc and a slight Jc increase in field. Using a combination of advanced transmission electron microscopy (TEM) techniques such as atomic resolution high-angle annular dark field scanning transmission electron microscopy, energy dispersive X-ray spectroscopy and electron energy-loss spectroscopy we have been able to decipher and characterize the effects of the Fe and Mn doping on the film architecture. The $YBaCuFeO_5$ anion-deficient double perovskite phase was detected in the form of 3D inclusions as well as epitaxially grown lamellas within the YBCO matrix. These nano-inclusions play a positive role as pinning centers responsible for the J_c/J_{sf} (H) dependency smoothening at high magnetic fields in the YBCO-MFO films with respect to the pristine YBCO films.

Introduction

High temperature superconducting materials have undergone a huge evolution over the past decades [1–5]. The second generation high temperature superconductors (2G HTS) or coated conductors (CC) are intended to be used partially along with, or instead of, the first generation HTC wires [6]. YBCO CC are being scaled to commercial lengths and are starting to be produced at an industrial scale [7]. These steps are only possible because of improved production processes and a better understanding of the materials architecture, micro- and nano-structure [8]. In order to enhance the performance of YBCO tapes in high magnetic fields, nanocomposites with different kinds of nanoprecipitates are produced (so-called nanostructured YBCO). The nanoprecipitates or the induced defects can act as pinning centers in order to enhance the pinning force and, consequently, the J_c values at high magnetic fields [3,9,10]. When YBCO films are produced by pulsed laser deposition (PLD), self-assembled nanoparticles and nanorods can be inserted into the YBCO matrix by the addition of foreign elements to the PLD target [11–17], but their size, distribution and density are strongly related to the deposition conditions and are not easy to tailor. Similarly, nanoparticles and nano-islands can also be formed in case of chemical solution deposition (CSD) of YBCO. Besides the relatively low cost of the CSD techniques for high critical current $YBa_2Cu_3O_7$ coated conductors [18], an advantage of CSD is the possibility to grow the pinning nanoparticles in two different ways: (i) from their precursor salts added directly to the YBCO precursor solution leading to the so-called “in-situ approach” [19–22] and (ii) by the addition of pre-formed nanoparticles to the YBCO precursor solution deriving in the so-called “ex-situ approach” [23–25]. Previous research has shown that achieving a tight control of nanoparticle nucleation and growth to avoid coalescence and coarsening when a single metalorganic precursor solution is used is a complex issue. Ex-situ nanoparticles, i.e. preformed nanoparticles which are mixed with the YBCO solution to form a colloidal system, provide options for an easier size control of the final nanostructure of the nanocomposites. However, this approach is, at the same time, more complex as it requires the particles to meet several criteria. First of all, they should have a well-defined size, secondly, agglomeration has to be avoided, and in the end the particles should be chemically stable at each step of the superconducting tape preparation process. The use of the ex-situ approach could open the door to a new nanocomposite approach which is just emerging [24]. For instance, magnetic nanoparticles could be introduced within the YBCO precursor solution after being synthesized ex-situ, which would allow to control and tune the properties of the nanoparticles beforehand. Several attempts have been made in the past to incorporate Fe-containing magnetic nanoparticles into the

YBCO matrix. Attempts using PLD deposition were in fact successful in producing materials without so-called Fe-poisoning of the YBCO, which is known to break down superconductivity by dropping T_c [26,27]. This effect can be decreased by adding Mn to YBCO, but the solubility of Mn appears to be very low [28,29]. No studies reporting a successful production of these materials by chemical deposition have been published so far.

In this work, we aim to characterize the unique microstructure of nanocomposite YBCO thin films on a $LaAlO_3$ (LAO) substrate, produced by spin coating from a standard YBCO-trifuluoroacetete (TFA) precursor solution enriched with pre-formed $MnFe_2O_4$ (MFO) nanoparticles, followed by pyrolysis and annealing steps. The complete structural characterization of this unique type of YBCO film is performed by atomic resolution high-angle annular dark field scanning transmission electron microscopy (HAADF-STEM), energy dispersive X-ray spectroscopy (EDX) and electron energy-loss spectroscopy (EELS), strongly focusing on the presence of the spinel nanoparticles in the YBCO film, the eventual dissolution of the spinel nanoparticles and the presence of separate Mn/Fe dopants or phases.

Methods

The $MnFe_2O_4$ nanoparticles were prepared following the solvothermal synthesis process as described by E. Solano et al. [30,31]. A bright field TEM image and X-ray diffraction (XRD) powder pattern of the $MnFe_2O_4$ spinel nanoparticles are shown in Fig. 1.

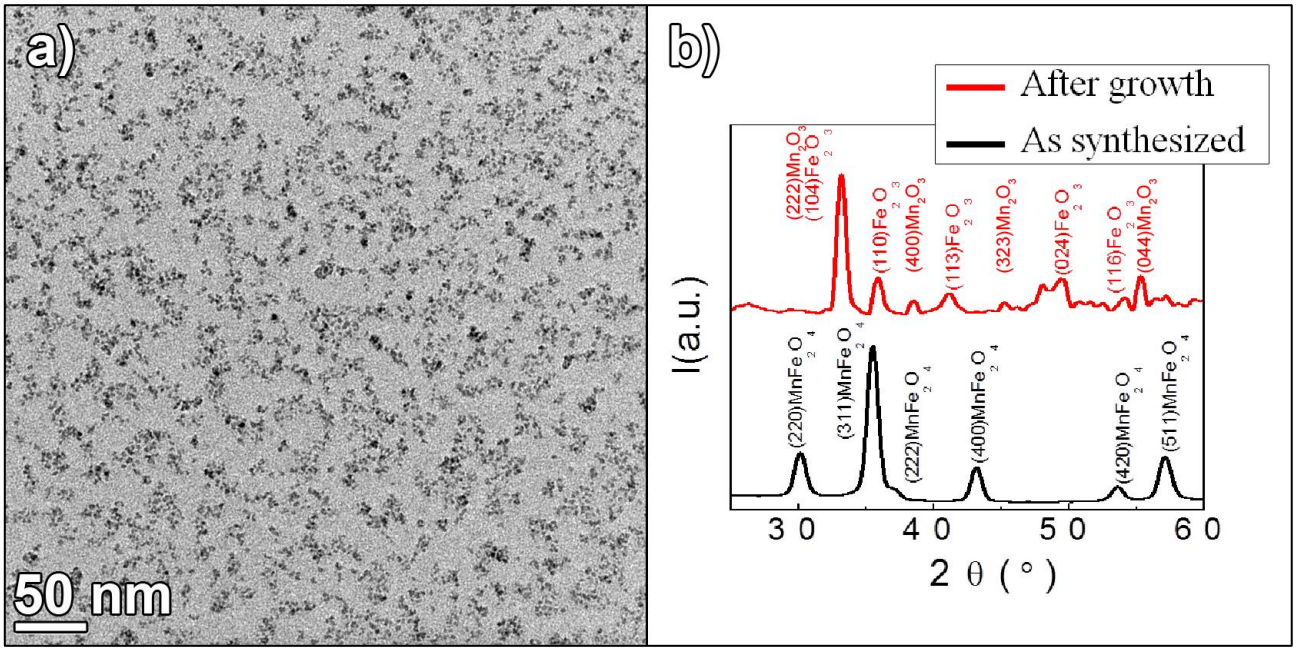

Figure 1. *Ex-situ nanoparticles.* a) BF TEM image showing 4-6 nm nanoparticles. No significant aggregates are observed. b) XRD patterns of as-synthesized $MnFe_2O_4$ powder (black curve) and $MnFe_2O_4$ powder subjected to the YBCO processing conditions (red curve).

3D YBCO nanocomposite films with 6 mol% of spinel $MnFe_2O_4$ nanoparticles are prepared following the chemical solution deposition (CSD) route. A 2 ml of 0,125 M YBCO with 6% $MnFe_2O_4$ nanoparticles solution is prepared by mixing 1 ml of a 0,25 M YBCO-TFA solution with 1 ml of 90 mM methanol colloidal solution of $MnFe_2O_4$ nanoparticles. This solution is deposited by spin-coating (6000 rpm, 2 min) over the pre-treated LAO substrate. The substrates are exposed to a thermal process in order to remove all possible remaining organic content and induce a surface reorganization that creates terraces, favoring the nucleation of new phases [32,33]. The processing conditions for the LAO substrate treatment are shown in Fig. S1. The resulting film is first subjected to a thermal treatment at low temperatures (pyrolysis) of 310ºC for 30 minutes to remove the organic content. The heating rate during the pyrolysis is kept at 3-5 K/min in the temperature range from 100ºC to 310ºC. Subsequently, the YBCO precursor layer is crystallized at 810 ºC in a humid N_2 – 0.02% O_2 flow for 3 hours. In the last stage the crystallized film is annealed at 210 ºC for 2 h in a dry oxygen atmosphere for 3.5 hours. The processing conditions for the pyrolysis and film growth are shown in Fig. S2 and S3 of the Supporting information.

The microstructure and phase analysis of the YBCO nanocomposite films were carried out by X-ray diffraction using a Bruker AXS GADDS diffractometer equipped with a 2D detector. The

critical temperature of the superconducting properties corresponding to T_c^{onset} and $J_c/J_c^{sf}(H)$ dependencies were measured by inductive measurements with a Superconducting Quantum Interference Device magnetometer (SQUID).

For TEM measurements, cross-section lamellas were produced by Focused Ion Beam (FIB-SEM, FEI Nova 600 Nanolab Dual Beam) as well as by Ar^+ ion milling, using a Gatan PIPS ion mill. High- and low-angle annular dark field scanning transmission electron microscopy (HAADF-STEM and LAADF STEM) imaging, STEM electron energy-loss spectroscopy (STEM-EELS) and STEM energy dispersive X-ray spectroscopy (STEM-EDX) experiments were performed on an FEI Titan "cubed" electron microscope, equipped with an aberration corrector for the probe-forming lens operated at 120/200/300 kV acceleration voltage. High resolution EELS experiments, using a Gatan Enfinium spectrometer were carried out with the electron monochromator excited to provide 250 meV energy resolution, using a convergence semi-angle of 18 mrad and a collection semi-angle β of 130 mrad. For EDX mapping a "Super-X" wide solid angle EDX detector was used at a voltage of 200kV. Bright field and high resolution transmission electron microscopy (BF TEM and HR TEM) was carried out using the Tecnai Osiris TEM operated at 200kV equipped with a "Super-X" EDX detector.

Results and discussion

A characterization of the nanoparticles powder is required in order to test their stability under the YBCO processing conditions. For that the powder nanoparticles, the solid precipitate obtained after the purification process is subjected to the same thermal treatment as the YBCO films: the pyrolysis and the growth processes (Fig. S2 and S3 of Supporting information). The XRD pattern of the nanoparticles powder after these thermal treatments reveals that the spinel $MnFe_2O_4$ phase decomposes producing a mixture of Fe_2O_3 and Mn_2O_3 (Fig. 1b), a behavior which strongly differs from that recently described for $CoFe_2O_4$ spinel nanoparticles [34]. Further investigation was therefore concentrated on the microstructural effects of the chemical interaction of these oxides with the YBCO matrix.

Nanocomposite superconductor architecture

The General Area Detector Diffraction System (GADDS) pattern (Fig. 2a) acquired from the obtained nanocomposite thin film material indicates a highly textured microstructure. Randomly oriented precipitates would introduce a ring in the pattern but this is not detected in this case. This is probably related, to the low concentration of these precipitates. No spinel $MnFe_2O_4$ peaks are observed in the XRD pattern (Fig. 2b).

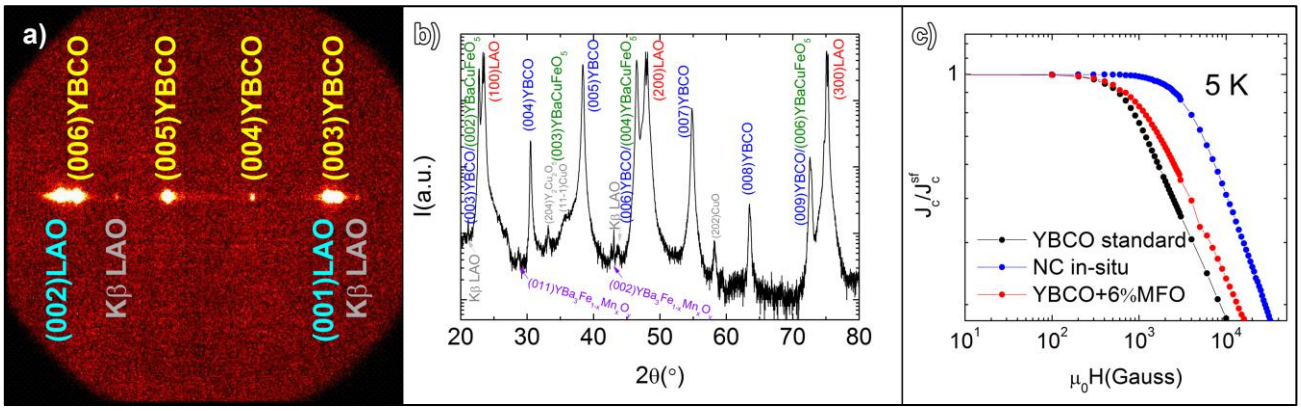

Figure 2. *Nanocomposite superconductor. XRD and J_c measurements.* a) 2D XRD θ-2θ pattern b) XRD spectrum of the nanocomposite on the LAO substrate. No signal of spinel nanoparticles is observed. c) J_c/J_c^{sf} (H) dependency of standard YBCO (black), the benchmark CSD nanocomposite[20,35] (blue) and the studied nanocomposite (red) at 5 K.

The resulting thin film nanocomposite demonstrates a T_c decrease down to values in the range of 65-80 K, varying from sample to sample, depending on the amount of Mn/Fe that is incorporated into the YBCO structure (this is later confirmed by EELS) [29]. The J_c/J_c^{sf} (H) dependency at 5K shows an increase of the critical current density normalized over the self-field compared to a standard YBCO film (Fig. 2c), but still lower than that of the YBCO-BYTO nanocomposite, which can be used as a benchmark [20,35]. The lowering of T_c and the moderate critical current density might be related to the interaction of YBCO with the $MnFe_2O_4$ decomposition products. To study the exact structure, composition and morphology of the film, TEM, EDX and EELS spectroscopy experiments were carried out.

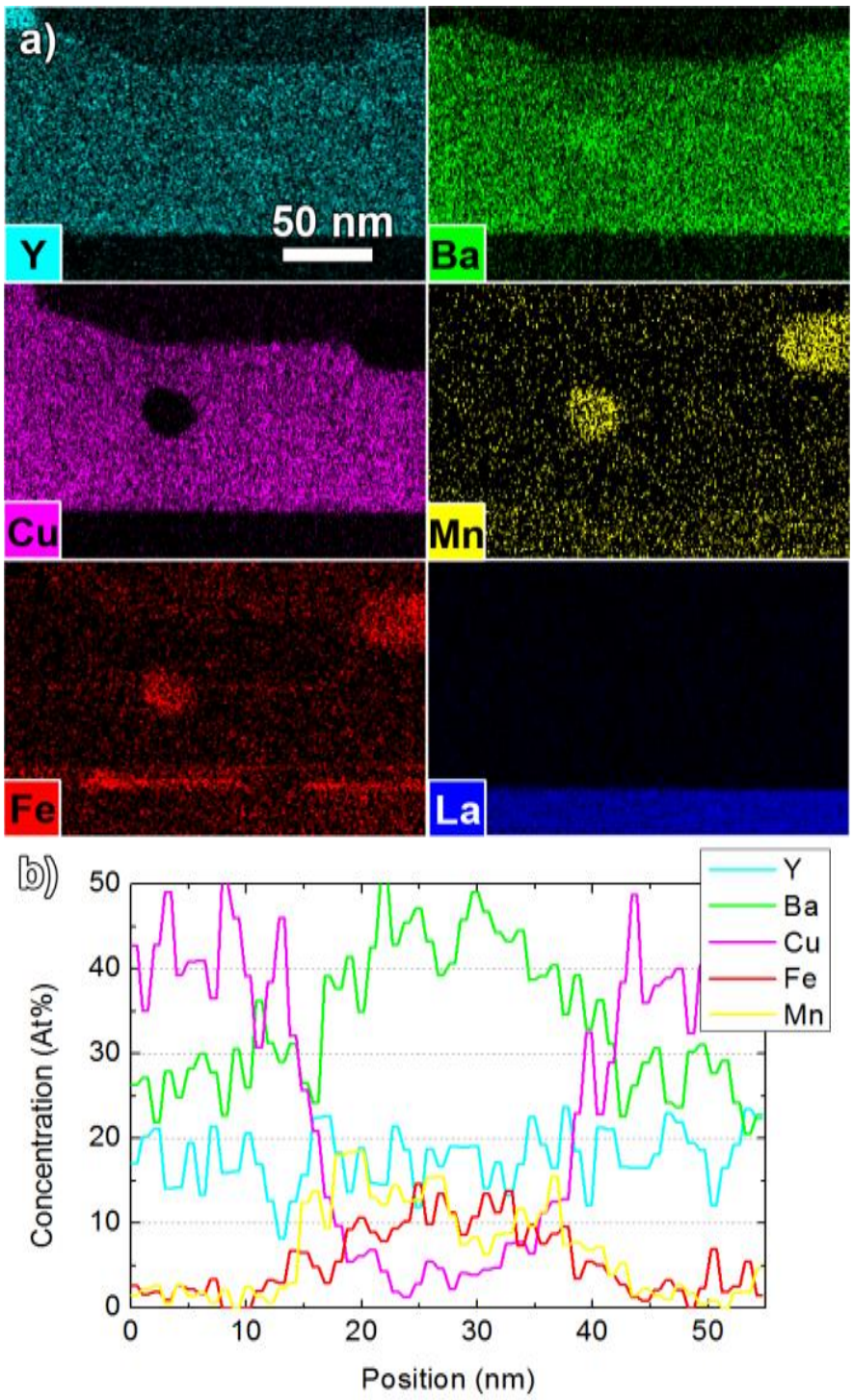

Figure 3. *Composition of the nanocomposite superconductor*. a) Overview EDX maps for Y, Ba, Cu, Fe, Mn and La. The present nanoparticles are $Ba_3YMnFeO_{9-\delta}$. The bottom part of the YBCO layer is Fe-doped. b) The integrated EDX signal profile across the $Ba_3YMnFeO_{9-\delta}$ nanoparticle in the center of figure a). The color-code is the same as in the EDX maps.

Overview EDX compositional maps of the YBCO film are displayed in Figure 3a. The thickness of the resulting thin film nanocomposite is ~110nm. No spinel $MnFe_2O_4$ nanoparticles are detected in the film. The map shows the presence of Mn-Fe-rich round-shaped inclusions, which also contain a high concentration of Ba and some Y, as demonstrated by the EDX signal profile in Fig. 3b. The EDX analysis reveals an average cation composition of these inclusions corresponding to Ba : Y : Fe : Mn = 3 : 1.1 : 0.7 : 1 (with standard deviations 0.1, 0.1, 0.1 and 0.05 respectively) measured on 6 different inclusion areas. Besides these inclusions, the Fe EDX map shows a clear tendency of Fe to segregate at the bottom of the YBCO layer in the proximity of the LAO interface.

Figure 4a shows a high resolution HAADF-STEM image of a Fe-Mn rich inclusion. The observed rectangular pattern of the cationic columns is characteristic of the perovskite structure with a cubic subcell parameter of ~4.2-4.3Å. The results of the EDX analysis (see above) suggest the $Ba_3YMnFeO_{9-\delta}$ composition of this perovskite phase (ABO_3), where the B-positions are jointly occupied by the Y, Mn and Fe cations. It should be noted that when a substantial anion deficiency is present ($\delta = 1.5$), the Y and transition metal cations form an ordered pattern as it is observed in the $Ba_3YFe_2O_{7.5}$ structure [36]. However, a higher oxygen content might promote cation disorder, as in the Y-doped $BaCoO_{3-\delta}$ perovskites [37]. Additionally, Mn co-doping can promote disorder as the tetrahedral oxygen coordination of a fraction of the B-cations in the $Ba_3YFe_2O_{7.5}$ structure is not very suitable for the Mn cations. The $Ba_3YMnFeO_{9-\delta}$ precipitates demonstrate a growth close to epitaxial on the LAO interface (Figure 4b), but a random orientation in the middle of the YBCO matrix. The size of the $Ba_3YMnFeO_{9-\delta}$ precipitates varies from 10 nm up to 80 nm..

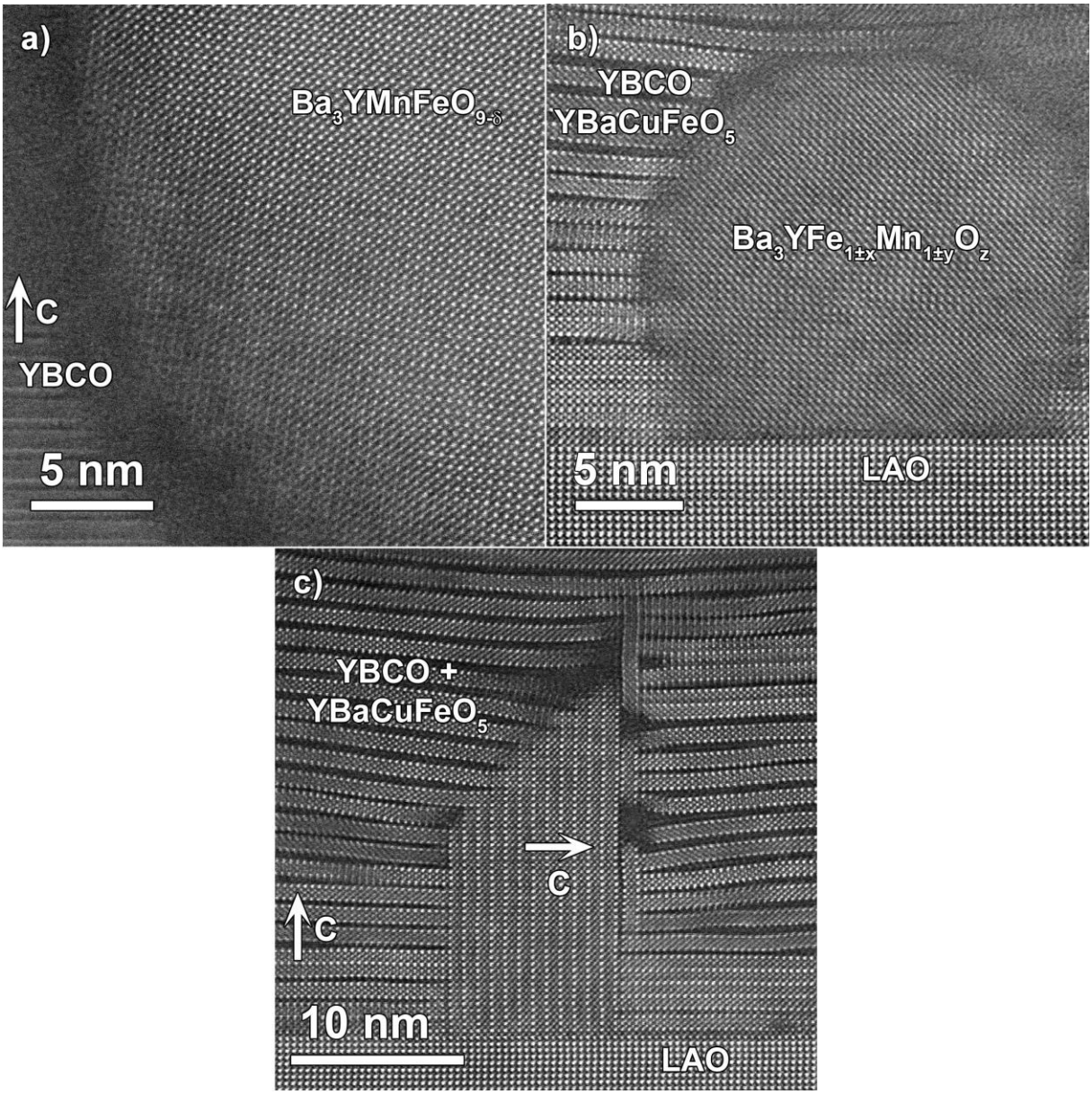

Figure 4. *Morphology of the nanocomposite superconductor*. High resolution HAADF-STEM Z-contrast images, showing the YBCO matrix together with a) a randomly oriented $Ba_3YMnFeO_{9-\delta}$ nanoparticle located in the middle of the YBCO matrix, b) a $Ba_3YMnFeO_{9-\delta}$ nanoparticle in an orientation close to epitaxial, located on the LAO substrate and c) a 90° rotated $YBaCuFeO_5$ grain on the LAO substrate

Figure 4c shows a HAADF-STEM image of the LAO-YBCO interface, demonstrating the presence of perovskite-like domains, clearly different from the YBCO structure. The EDX spectra recorded from these domains confirm the presence of Y, Ba, Cu and Fe, although an exact quantification is impossible due to the interference with the YBCO matrix. It will be demonstrated by atomic resolution EDX mapping that these domains possess the A-site ordered double perovskite structure of the $YBaCuFeO_5$ phase [38]. The vast majority of such double perovskite $YBaCuFeO_5$-like grains with a size of 20 to 100 nm are located near the LAO/YBCO interface, in accordance with the Fe distribution in the EDX maps in Fig.3a. The YBCO film and the double perovskite phase exhibit an epitaxial growth character with mainly the following epitaxial relationship:

$$[001]_{YBCO,\ YBaCuFeO_5} // [001]_{LAO}$$

$$[010], [100]_{YBCO,\ YBaCuFeO_5} // [100]_{LAO}$$

However, a few grains nucleated with the c-axis parallel to the substrate were also observed (see Figure 4c). The appearance of such grains is a common issue when the supersaturation degree is too high [39,40]. The epitaxial relationship is then:

$$[100]_{YBCO,\ YBaCuFeO_5} // [001]_{LAO}$$

In that case, the (00l) planes of YBCO are strongly buckled around the interfaces in order to release the stress generated by the lattice mismatch among perpendicularly oriented grains.

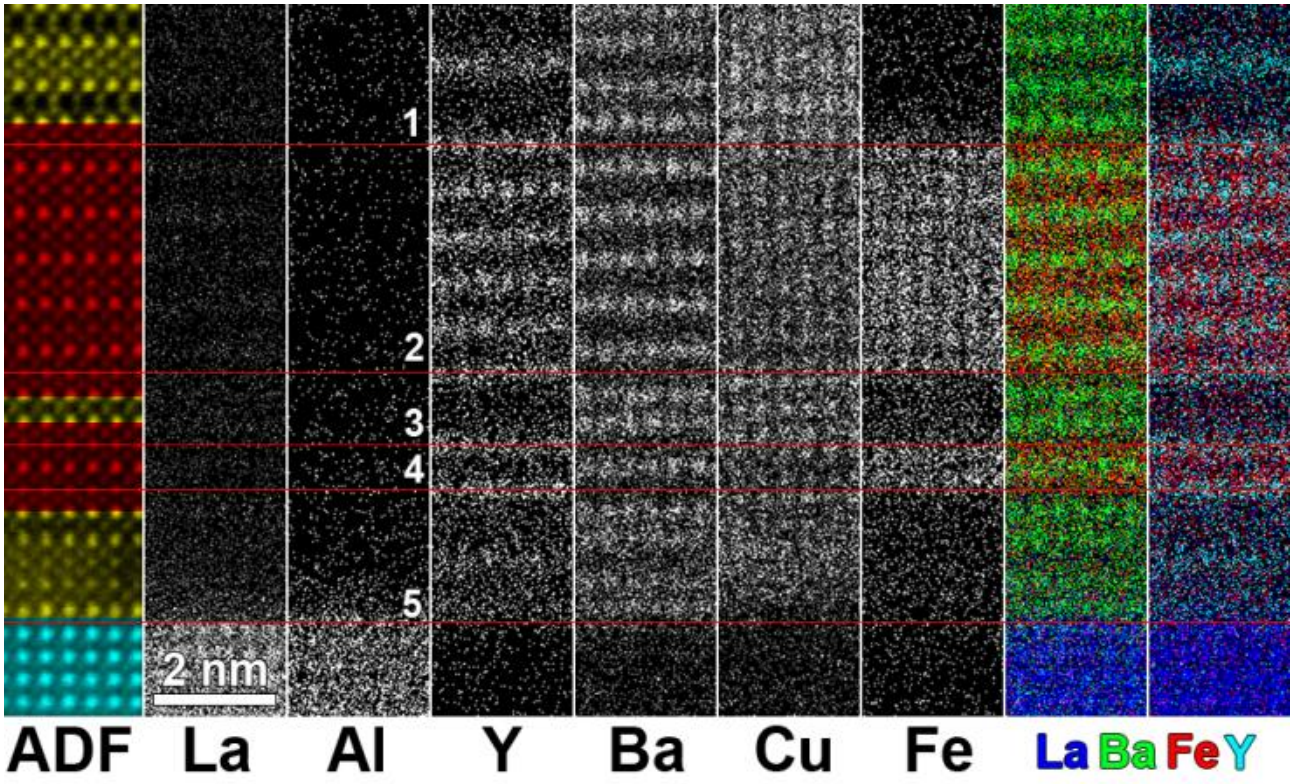

Figure 5. *Double perovskite $YBaCuFeO_5$ intergrowths in the nanocomposite superconductor*. HAADF-STEM image and atomic-resolution EDX maps of the film/substrate interface (similar to the region shown in Fig. 4c), showing the presence of Y123 & Y124 (yellow) and the double perovskite phase (red) on top of the LAO substrate (cyan). Red lines mark the terminating planes of the indicated phases; 1–4: YO planes terminating the double perovskite phases which contain mixed Fe/Cu sites; 5: last AlO_2 plane of LAO substrate.

Atomic resolution EDX maps of the $YBaCuFeO_5$-like domains reveal an ordered alternation of the Y and Ba layers in the A positions, whereas Cu and Fe are distributed randomly (Fig. 5). This double perovskite phase can be present as separate 3D domains, but can also appear as lamellas of different thickness in the YBCO matrix. STEM-EELS atomic resolution maps (Fig. 6a) with a monochromatic electron source (ΔE = 250 meV) also show that Fe partially replaces Cu in the YBCO structure A clear Fe $L_{2,3}$ edge is present in the EELS spectrum acquired from the double perovskite phase (1st spectrum in Fig. 6b), confirming the high Fe content there. No Mn signal, neither by EDX nor by EELS, is observed in the YBCO matrix or double perovskite. On top of the Fe measured in the double perovskite, a small Fe $L_{2,3}$ signal is also present in the YBCO region (2nd spectrum in Fig. 6b). This means that some Fe is also incorporated in the YBCO structure, poisoning the superconducting properties and causing the observed decrease of T_c as it was reported in

previous works [29]. The absence of a chemical shift between the Fe L_3 for Fe in the double perovskite structure and Fe in the YBCO (inset) indicates that both should have a similar valency.

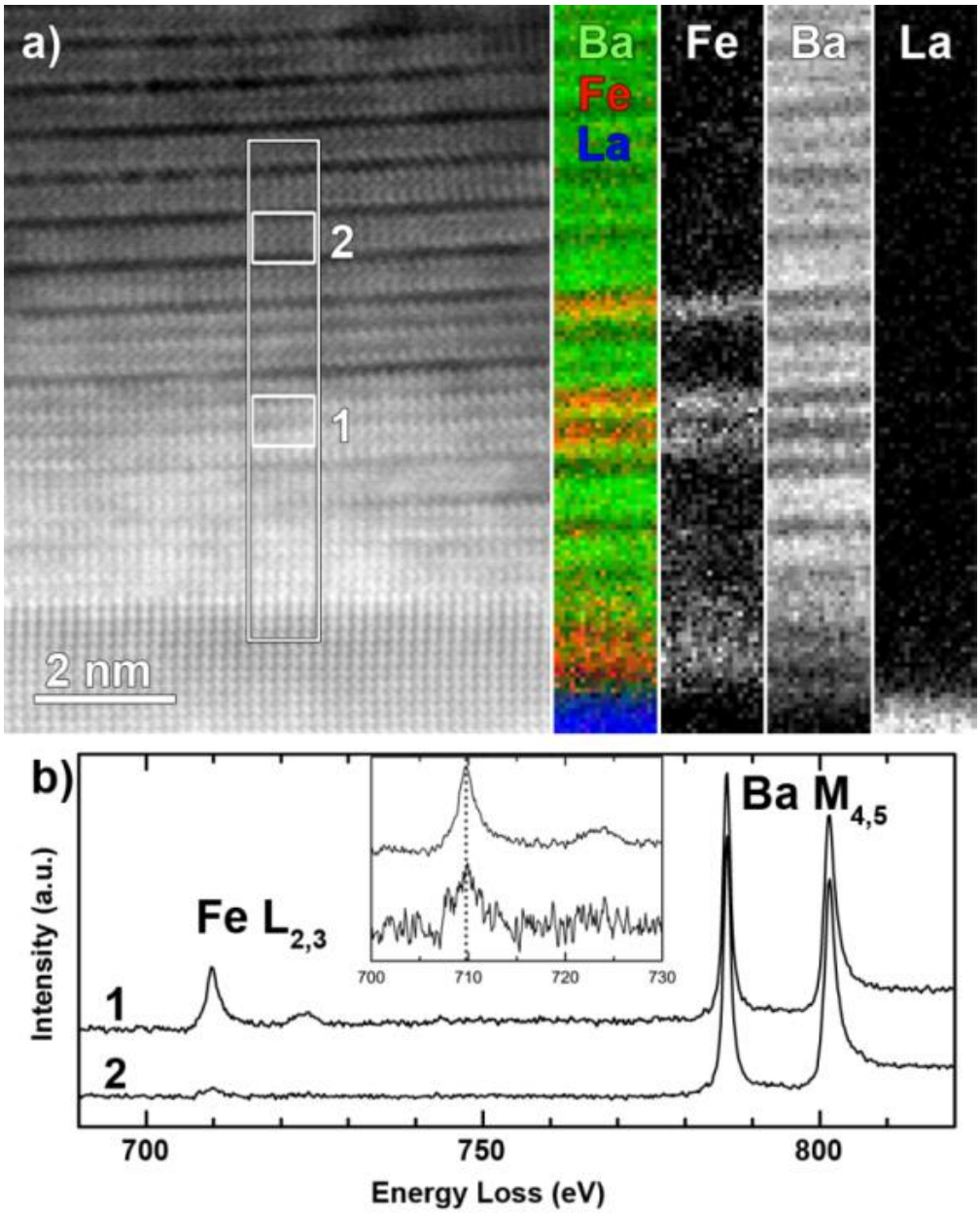

Figure 6. *Fe doping and double perovskite $YBaCuFeO_5$ intergrowths in the nanocomposite superconductor.* a) HAADF-STEM image and atomic-resolution EELS maps of the thin film/substrate interface. b) Averaged EELS spectra from the areas indicated in a). 1 – Double perovskite, 2 – Fe:YBCO. The spectra are scaled to the integral Ba $M_{4,5}$ edge intensity. Inset; Fe $L_{2,3}$ edge spectra scaled from the two regions scaled to the Fe $L_{2,3}$ edge intensity. The dotted line indicates the Fe L_3 edge maximum.

The formation of the double perovskite $YBaCuFeO_5$-like inclusions and partial Fe for Cu replacement in the YBCO matrix creates an excess of Cu in comparison to the stoichiometric $YBa_2Cu_3O_7$ composition. This excess Cu is accommodated in the abundant planar defects related to the formation of double and triple chains of edge-sharing CuO_4 squares, which can be considered as the insertion of Y124 or Y125 lamellas. Actually, lamellas of double perovskite, Y124, Y125 and YBCO are closely intermixed inducing a local deformation of the YBCO matrix and buckling of the YBCO blocks in the vicinity of the interface (Fig. 4c).

Conclusions

We have studied the structural and superconducting properties of YBCO nanocomposite films prepared by an ex-situ approach using $MnFe_2O_4$ nanoparticles. The results reveal that the $MnFe_2O_4$ nanoparticles decompose and react with the YBCO precursors causing the presence of separate Mn/Fe dopants or phases. The chemical instability of the ex-situ nanoparticles during the synthesis leads to the formation of several types of inclusions in the superconductor film. Firstly, $YBaCuFeO_5$ double perovskite phase intergrowths are observed next to the LAO substrate. Secondly, Fe-doping of YBCO takes place leading to a decrease of Tc. Finally, $Ba_3YFeMnO_{9-\delta}$ nanoinclusions are present. Together with the short double and triple CuO-chain layer intergrowths the newly formed nanoinclusions can serve as the artificial pinning centers in the coated conductor film. Cultivation of such pinning centers is promising for J_c/J_{sf} enhancement at high magnetic fields, but $MnFe_2O_4$ spinel nanoparticles are not ideal as they decompose during the growth process of the film.

Acknowledgements

The authors gratefully acknowledge Prof. Dr. A. Abakumov and Dr. J. Gazquez for discussions and corrections. Part of this work was performed within the framework of the EUROTAPES project (FP7-NMP.2011.2.2-1 Grant no. 280432), funded by the European Union. ICMAB research was financed by the Ministry of Economy and Competitiveness, and FEDER funds under the projects MAT2011-28874-C02-01, MAT2014-51778-C2-1-R, ENE2014-56109-C3-3-R and Consolider Nanoselect CSD2007-00041, and by Generalitat de Catalunya (2009 SGR 770, 2015 SGR 753 and Xarmae). ICMAB acknowledges support from Severo Ochoa Program (MINECO, Grant SEV-2015-0496).

References

[1] Larbalestier D, Gurevich A, Feldmann D M and Polyanskii A 2001 High-Tc superconducting materials for electric power applications *Nature* **414** 368–377

[2] Gutierrez J, Llordes A, Gazquez J, Gibert M, Roma N, Ricart S, Pomar A, Sandiumenge F, Mestres N, Puig T and Obradors X 2007 Strong isotropic flux pinning in solution-derived YBa2Cu3O7-x nanocomposite superconductor films *Nat Mater* **6** 367–373

[3] Llordés A, Palau A, Gázquez J, Coll M, Vlad R, Pomar A, Arbiol J, Guzmán R, Ye S, Rouco V, Sandiumenge F, Ricart S, Puig T, Varela M, Chateigner D, Vanacken J, Gutiérrez J, Moshchalkov V, Deutscher G, Magen C and Obradors X 2012 Nanoscale strain-induced pair suppression as a vortex-pinning mechanism in high-temperature superconductors *Nat Mater* **11** 329–336

[4] Obradors X and Puig T 2014 Coated conductors for power applications: materials challenges *Superconductor Science and Technology* **27** 044003

[5] Uchida S 2014 *High Temperature Superconductivity: The Road to Higher Critical Temperature* vol 213 (Springer)

[6] Rupich M W, Li X, Thieme C, Sathyamurthy S, Fleshler S, Tucker D, Thompson E, Schreiber J, Lynch J, Buczek D, DeMoranville K, Inch J, Cedrone P and Slack J 2010 Advances in second generation high temperature superconducting wire manufacturing and R&D at American Superconductor Corporation *Superconductor Science and Technology* **23** 014015

[7] Shiohara Y, Yoshizumi M, Takagi Y and Izumi T 2013 Future prospects of high Tc superconductors-coated conductors and their applications *Physica C: Superconductivity* **484** 1–5

[8] Goyal A 2004 *Second-generation HTS conductors* (Springer Science & Business Media)

[9] Maiorov B, Baily S A, Zhou H, Ugurlu O, Kennison J A, Dowden P C, Holesinger T G, Foltyn S R and Civale L 2009 Synergetic combination of different types of defect to optimize pinning landscape using BaZrO3-doped YBa2Cu3O7 *Nat Mater* **8** 398–404

[10] Gazquez J, Guzman R, Mishra R, Bartolomé E, Salafranca J, Magén C, Varela M, Coll M, Palau A, Valvidares S M, Gargiani P, Pellegrin E, Herrero-Martin J, Pennycook S J, Pantelides S T, Puig T and Obradors X 2016 Emerging Diluted Ferromagnetism in High-Tc Superconductors Driven by Point Defect Clusters *Advanced Science* n/a–n/a

[11] Varanasi C V, Barnes P N, Burke J, Brunke L, Maartense I, Haugan T J, Stinzianni E A, Dunn K A and Haldar P 2006 Flux pinning enhancement in YBa2Cu3O 7− x films with BaSnO 3 nanoparticles *Superconductor Science and Technology* **19** L37

[12] Harrington S A, Durrell J H, Maiorov B, Wang H, Wimbush S C, Kursumovic A, Lee J H and MacManus-Driscoll J L 2009 Self-assembled, rare earth tantalate pyrochlore nanoparticles for

superior flux pinning in YBa2Cu3O7−δ films *Superconductor Science and Technology* **22** 022001

[13] Feldmann D M, Holesinger T G, Maiorov B, Foltyn S R, Coulter J Y and Apodaca I 2010 Improved flux pinning in YBa2Cu3O7 with nanorods of the double perovskite Ba2YNbO6 *Superconductor Science and Technology* **23** 095004

[14] Opherden L, Sieger M, Pahlke P, Hühne R, Schultz L, Meledin A, Van Tendeloo G, Nast R, Holzapfel B, Bianchetti M, MacManus-Driscoll J L and Hänisch J 2016 Large pinning forces and matching effects in YBa2Cu3O7-δ thin films with Ba2Y(Nb/Ta)O6 nano-precipitates *Scientific Reports* **6** 21188–

[15] Pahlke P, LAO M, Eisterer M, Meledin A, Tendeloo G V, Hanisch J, Sieger M, Usoskin A, Stromer J, Holzapfel B, Schultz L and Huhne R 2016 Reduced Jc anisotropy and enhanced in-field performance of thick BaHfO3-doped YBa2Cu3O7-δ films on ABAD-YSZ templates *IEEE Transactions on Applied Superconductivity* **PP** 1–1

[16] Rizzo F, Augieri A, Angrisani Armenio A, Galluzzi V, Mancini A, Pinto V, Rufoloni A, Vannozzi A, Bianchetti M, Kursumovic A, MacManus-Driscoll J L, Meledin A, Van Tendeloo G and Celentano G 2016 Enhanced 77 K vortex-pinning in YBa2Cu3O7−x films with Ba2Y TaO6 and mixed Ba2Y TaO6 + Ba2Y NbO6 nano-columnar inclusions with irreversibility field to 11 T *APL Mater.* **4**

[17] Sieger M, Pahlke P, Hanisch J, Sparing M, Bianchetti M, MacManus-Driscoll J, Lao M, Eisterer M, MELEDIN A, Tendeloo G V, Nast R, Schultz L, Holzapfel B and Huhne R 2016 Ba2Y(Nb/Ta)O6-doped YBCO films on biaxially textured Ni-5at.% W substrates *IEEE Transactions on Applied Superconductivity* **PP** 1–1

[18] Obradors X, Puig T, Pomar A, Sandiumenge F, Piñol S, Mestres N, Castaño O, Coll M, Cavallaro A, Palau A, Gázquez J, González J C, Gutiérrez J, Romà N, Ricart S, Moretó J M, Rossell M D and Tendeloo G van 2004 Chemical solution deposition: a path towards low cost coated conductors *Superconductor Science and Technology* **17** 1055

[19] Pomar A, Vlad V R, Llordes A, Palau A, Gutierrez J, Ricart S, Puig T, Obradors X and Usoskin A 2009 Enhanced vortex pinning in YBCO coated conductors with BZO nanoparticles from chemical solution deposition *Applied Superconductivity, IEEE Transactions on* **19** 3258–3261

[20] Coll M, Guzman R, Garcés P, Gazquez J, Rouco V, Palau A, Ye S, Magen C, Suo H, Castro H, Puig T and Obradors X 2014 Size-controlled spontaneously segregated Ba2YTaO6 nanoparticles in YBa2Cu3O7 nanocomposites obtained by chemical solution deposition *Superconductor Science and Technology* **27** 044008

[21] Erbe M, Hänisch J, Hühne R, Freudenberg T, Kirchner A, Molina-Luna L, Damm C, Tendeloo G V, Kaskel S, Schultz L and Holzapfel B 2015 BaHfO3 artificial pinning centres in TFA-MOD-derived YBCO and GdBCO thin films *Superconductor Science and Technology* **28** 114002

[22] Molina-Luna L, Duerrschnabel M, Turner S, Erbe M, Martinez G T, Aert S V, Holzapfel B and Tendeloo G V 2015 Atomic and electronic structures of BaHfO3 -doped TFA-MOD-derived YBa2Cu3O7−δ thin films *Superconductor Science and Technology* **28** 115009

[23] Bretos I, Schneller T, Falter M, Backer M, Hollmann E, Wordenweber R, Molina-Luna L, Van Tendeloo G and Eibl O 2015 Solution-derived YBa2Cu3O7−δ (YBCO) superconducting films with BaZrO3 (BZO) nanodots based on reverse micelle stabilized nanoparticles *J. Mater. Chem. C* **3** 3971–3979

[24] Cayado P, Keukeleere K D, Garzón A, Perez-Mirabet L, Meledin A, Roo J D, Vallés F, Mundet B, Rijckaert H, Pollefeyt G, Coll M, Ricart S, Palau A, Gázquez J, Ros J, Tendeloo G V, Driessche I V, Puig T and Obradors X 2015 Epitaxial YBa 2 Cu 3 O 7− x nanocomposite thin films from colloidal solutions *Superconductor Science and Technology* **28** 124007

[25] De Keukeleere K, Cayado P, Meledin A, Vallès F, De Roo J, Rijckaert H, Pollefeyt G, Bruneel E, Palau A, Coll M, Ricart S, Van Tendeloo G, Puig T, Obradors X and Van Driessche I 2016 Superconducting YBa2Cu3O7–δ Nanocomposites Using Preformed ZrO2 Nanocrystals: Growth Mechanisms and Vortex Pinning Properties *Advanced Electronic Materials*

[26] Wimbush S C, Durrell J H, Bali R, Yu R, Wang H, Harrington S . and MacManus-Driscoll J L 2009 Practical Magnetic Pinning in YBCO *Applied Superconductivity, IEEE Transactions on* **19** 3148–3151

[27] Wimbush S C, Durrell J H, Tsai C F, Wang H, Jia Q X, Blamire M G and MacManus-Driscoll J L 2010 Enhanced critical current in YBa 2 Cu 3 O 7−δ thin films through pinning by ferromagnetic YFeO 3 nanoparticles *Superconductor Science and Technology* **23** 045019–

[28] Regnier S, Alfred-Duplan C, Vacquier G and Marfaing J 1996 Effect of Mn inclusion in superconducting YBCO-based composites *Applied Superconductivity* **4** 41–51

[29] Skakle J M S 1998 Crystal chemical substitutions and doping of YBa2Cu3Ox and related superconductors *Materials Science and Engineering: R: Reports* **23** 1–40

[30] Solano E, Perez-Mirabet L, Martinez-Julian F, Guzmán R, Arbiol J, Puig T, Obradors X, Yañez R, Pomar A, Ricart S and Ros J 2012 Facile and efficient one-pot solvothermal and microwave-assisted synthesis of stable colloidal solutions of MFe2O4 spinel magnetic nanoparticles *Journal of Nanoparticle Research* **14** 1–15

[31] Solano Minuesa E 2014 *Synthesis and characterisation of ferrite nanoparticles for* $YBa_2Cu_3O_7$ (Universitat Autònoma de Barcelona)

[32] Huijbregtse J ., Rector J . and Dam B 2001 Effect of the two (1 0 0) SrTiO3 substrate terminations on the nucleation and growth of YBa2Cu3O7−δ thin films *Physica C: Superconductivity* **351** 183–199

[33] Sánchez F, Ocal C and Fontcuberta J 2014 Tailored surfaces of perovskite oxide substrates for conducted growth of thin films *Chemical Society Reviews* **43** 2272–2285

[34] Bartolome E, Cayado P, Solano E, Ricart S, Gazquez J, Mundet B, Coll M, Puig T, Obradors X, Valvidares M, Herrero-Martin J, Gargiani P and Pellegrin E 2016 Magnetic stability against calcining of microwave-synthesized CoFe2O4 nanoparticles *New J. Chem.*

[35] Coll M, Ye S, Rouco V, Palau A, Guzman R, Gazquez J, Arbiol J, Suo H, Puig T and Obradors X 2013 Solution-derived YBa2Cu3O7 nanocomposite films with a Ba2YTaO6 secondary phase for improved superconducting properties *Superconductor Science and Technology* **26** 015001

[36] Kudryavtsev D, Mill B, Vedernikov N and Shaplygin I 1992 New compounds in the Ln2O3-BaO-Fe2O3+δ systems *Inorganic materials* **28** 943–946

[37] Lomakov M V, Istomin S Y, Abakumov A M, Tendeloo G V and Antipov E V 2008 Synthesis and characterization of oxygen-deficient oxides BaCo1 − xYxO3 − y, x = 0.15, 0.25 and 0.33, with the perovskite structure *Solid State Ionics* **179** 1885–1889

[38] Caignaert V, Mirebeau I, Bourée F, Nguyen N, Ducouret A, Greneche J-M and Raveau B 1995 Crystal and Magnetic Structure of YBaCuFeO5 *Journal of Solid State Chemistry* **114** 24–35

[39] Obradors X, Puig T, Ricart S, Coll M, Gazquez J, Palau A and Granados X 2012 Growth, nanostructure and vortex pinning in superconducting YBa 2 Cu 3 O 7 thin films based on trifluoroacetate solutions *Superconductor Science and Technology* **25** 123001

[40] Obradors X, Martínez-Julián F, Zalamova K, Vlad V R, Pomar A, Palau A, Llordés A, Chen H, Coll M, Ricart S, Mestres N, Granados X, Puig T and Rikel M 2012 Nucleation and mesostrain influence on percolating critical currents of solution derived {YBa2Cu3O7} superconducting thin films *Physica C: Superconductivity* **482** 58–67